

## Tuning Single-Molecule Dynamics in Functionalized Mesoporous Silica

Timo Lebold,<sup>[a, d]</sup> Lea A. Mühlstein,<sup>[a, d]</sup> Julia Blechinger,<sup>[a]</sup> Melanie Riederer,<sup>[a]</sup> Heinz Amenitsch,<sup>[b]</sup> Ralf Köhn,<sup>[a]</sup> Kalina Peneva,<sup>[c]</sup> Klaus Müllen,<sup>[c]</sup> Jens Michaelis,<sup>[a]</sup> Christoph Bräuchle,<sup>\*[a]</sup> and Thomas Bein<sup>\*[a]</sup>

**Abstract:** Mesoporous silica materials are promising host structures for diverse applications in nanoscience. Many applications can profit significantly from the ability to influence guest dynamics in the host matrix. To this end, we introduce covalently attached organic functionalization into the walls of mesoporous silica networks. Using single-molecule fluorescence microscopy, we study the diffusion behavior of single terrylene diimide dye molecules in functionalized mesoporous silica films. We show that,

through variation of the chemical nature and density of the functional groups, the diffusion dynamics of the dye molecules, in the presence of the surfactant template, can be controlled precisely. The mean diffusion coefficient of the dye molecules increases or decreases depending on the functional

group attached to the silica wall. This allows fine-tuning of the diffusion dynamics of the dye by approximately one order of magnitude. The observed changes in the mean diffusion coefficients can be explained by shielding of hydroxyl groups on the silica surface in combination with changes in the rigidity of the micellar packing in the film, as well as direct interactions between the functional groups and the dye molecules.

**Keywords:** diffusion • host–guest systems • mesoporous materials • self-assembly • single-molecule studies

### Introduction

Surfactant-templated, periodic mesoporous materials<sup>[1]</sup> are highly versatile hosts for diverse guest molecules, owing to their large surface areas, tunable pore sizes (about 2–15 nm

in diameter) and pore topologies, and well-defined surface properties. These attractive pore systems have been used for numerous applications including molecular and cluster-based catalysis,<sup>[2]</sup> selective sequestration of contaminants<sup>[3]</sup> and chromatography,<sup>[4]</sup> stabilization of conducting nanoscale wires,<sup>[5]</sup> and as novel drug-delivery systems.<sup>[6]</sup> For many of these applications, the mesoporous materials are expected to show enhanced properties when their inner channel walls are functionalized with organic moieties to fine-tune host–guest interactions. This is particularly important for drug-delivery systems that require the drug to be released at a slow rate in order to generate a desired depot effect.<sup>[7]</sup>


Three principal methods have been developed for organic functionalization of mesoporous materials. The first is the so-called post-synthesis grafting method.<sup>[8]</sup> For this approach, the pre-synthesized silica material is modified with alkoxy or chloro organosilanes.<sup>[9]</sup> An alternative approach is based on direct post-synthetic substitution of silica with organometallic compounds.<sup>[10]</sup> Finally, organic modification of mesoporous silica can be achieved by copolymerization of an organosilane with a silica precursor in the presence of the surfactant template.<sup>[11]</sup> This process is called co-condensation.<sup>[12]</sup> In this study, the co-condensation method was

[a] T. Lebold, L. A. Mühlstein, J. Blechinger, M. Riederer, Dr. R. Köhn, Prof. Dr. J. Michaelis, Prof. Dr. C. Bräuchle, Prof. Dr. T. Bein  
Department of Chemistry and Biochemistry and Center for Nanoscience (CeNS)  
Ludwig-Maximilians-Universität München (LMU)  
Butenandtstrasse 5-13 (E), 81377 Munich (Germany)  
Fax: (+49) 89-2180-77622  
E-mail: Christoph.Braeuchle@cup.uni-muenchen.de  
bein@lmu.de

[b] Dr. H. Amenitsch  
Institute of Biophysics and Nanosystems Research  
Austrian Academy of Sciences  
Schmidlstrasse 6, 8042 Graz (Austria)

[c] K. Peneva, Prof. Dr. K. Müllen  
Max-Planck-Institute for Polymer Research  
Ackermannweg 10, 55128 Mainz (Germany)

[d] T. Lebold, L. A. Mühlstein  
These authors contributed equally to this work.

 Supporting information for this article is available on the WWW under <http://dx.doi.org/10.1002/chem.200801380>.

used as it enables homogenous incorporation of functional groups into the walls of the mesoporous films.

Transport of guest molecules in the channels is of paramount importance for the functionality of these materials. Ensemble diffusion of guest molecules in porous systems has been studied by pulsed field-gradient NMR spectroscopy<sup>[13]</sup> and neutron scattering.<sup>[14]</sup> Fluorescence correlation spectroscopy (FCS) has been applied widely to study the diffusion of dye molecules in liquids,<sup>[15]</sup> porous media,<sup>[16]</sup> biological systems,<sup>[17]</sup> and recently in ordered mesoporous hosts.<sup>[18]</sup> However, with this technique individual trajectories cannot be determined, and heterogeneities may be difficult to extract. A complete understanding of the dynamics of guest species inside the pores can be gained by single-molecule fluorescence microscopy. We recently showed that this technique can be used to track individual dye molecules inside mesoporous silica thin films.<sup>[19]</sup> The resulting trajectories give a detailed picture of the structure and connectivity of different pore systems and allow us to analyze the dynamics of guests inside mesoporous hosts.

Here we show that organic functionalization of mesoporous thin films has a profound influence on the dynamics of individual guest molecules inside the porous network.

## Results and Discussion

**Characterization:** The functionalized mesoporous thin films were characterized by a range of methods to determine the pore structure and the nature of the functionalization.

One-dimensional (1D) X-ray-diffractograms (Figure 1) indicate that the mesoporous films exhibit 2D hexagonal order; that is, the amorphous silica surrounding the Brij micelles forms hexagonally packed cylindrical pores parallel to the substrate.<sup>[19c]</sup> The pore-to-pore distance decreases with increasing length of the functional group (Figure 1a) and with increasing functional-group density (Figure 1b–d).

In addition, grazing-incidence small-angle X-ray scattering (GISAXS) patterns of selected samples were recorded (Figure 1e–g). These data confirm that the mesoporous films exhibit 2D hexagonal order. The elliptical shape of the hexagonal pattern is due to shrinkage perpendicular to the glass surface owing to drying effects resulting in elliptically shaped pores.<sup>[20]</sup> The pore-to-pore distances,  $a$  values, and percentage of shrinkage are shown in Table 1.

As only the (10) reflection can be seen in 1D X-ray diffractograms, the values calculated for the pore-to-pore distance from those experiments must be compared to the  $a(10)$  value obtained from the GISAXS patterns. The values obtained from 1D XRD experiments are in good agreement with those

calculated from the GISAXS patterns (Table 1).

Raman spectra of functionalized mesoporous silica synthesized in anodic alumina membranes were recorded to confirm incorporation of the functional groups. By using this method, it is possible to identify cyanopropyl and phenyl functionalization (Figure 2). It is not possible to prove successful alkyl functionalization because the C–H vibrations of the functional groups overlap with those of the Brij template.

Alkyl functionalization can be detected in the solid-state <sup>13</sup>C NMR spectra of the functionalized mesoporous silica synthesized in anodic alumina membranes. The relevant signals (SiCH<sub>3</sub>, SiCH<sub>2</sub>CH<sub>3</sub>, and SiCH<sub>2</sub>CH<sub>2</sub>CH<sub>3</sub>) are indicated in Figure 3 by arrows (the adjacent number refers to the number of C atoms in the functional group). Furthermore, it is possible to gain information about the conformation of the alkyl chains of the Brij template from the <sup>13</sup>C NMR spectra. It has been reported that the presence of the *gauche* conformation in longer *n*-alkyl chains results in a shift of the <sup>13</sup>C NMR signal by 3 or 4 ppm to lower values compared to the *trans* conformation.<sup>[21]</sup> Thus the signal labeled # stems from the *trans* conformation of the alkyl chain of the template and the signal labeled with an asterisk originates from the *gauche* conformation (Figure 3). Although it is difficult to derive absolute quantitative information from the NMR signals because the spectra were recorded in cross-polarization mode, it is possible to compare the relative intensity of the *trans* and the *gauche* signals. In Figure 3a, it can be seen that the intensity of the *trans* signal decreases compared to that of the *gauche* signal with increasing concentration of the phenyl group. Similarly, with increasing length of the alkyl groups, the ratio of *trans* to *gauche* signal decreases (Figure 3b). This shows that increasing functional-group density and increasing the length of the alkyl group causes a higher degree of disorder of the alkyl chains of the template molecules.

**Single-molecule trajectories:** In this study we focus on the influence of functional groups on the diffusion of an incorporated guest molecule. In this context single-molecule approaches prevail over classical ensemble techniques, as they offer direct insights into mechanistic details of the interaction of the guest with the host matrix. Thus, DIP-TDI dye

Table 1. The  $a$  values obtained from 1D X-ray diffraction data as well as  $a$  values and lateral shrinkage calculated from GISAXS patterns.

Sample	$a(10)$ [nm] from 1D-XRD	$a(10)$ [nm] from GISAXS	$a(01)$ [nm] from GISAXS	Shrinkage [%] from GISAXS
10 mol% methyl	5.9	–	–	–
10 mol% ethyl	5.6	–	–	–
10 mol% propyl	5.5	5.4	5.7	20
5.0 mol% cyanopropyl	6.2	–	–	–
10 mol% cyanopropyl	6.0	–	–	–
20 mol% cyanopropyl	5.9	5.9	6.2	14
5.0 mol% phenyl	5.9	–	–	–
10 mol% phenyl	5.8	–	–	–
20 mol% phenyl	5.5	5.4	5.8	22

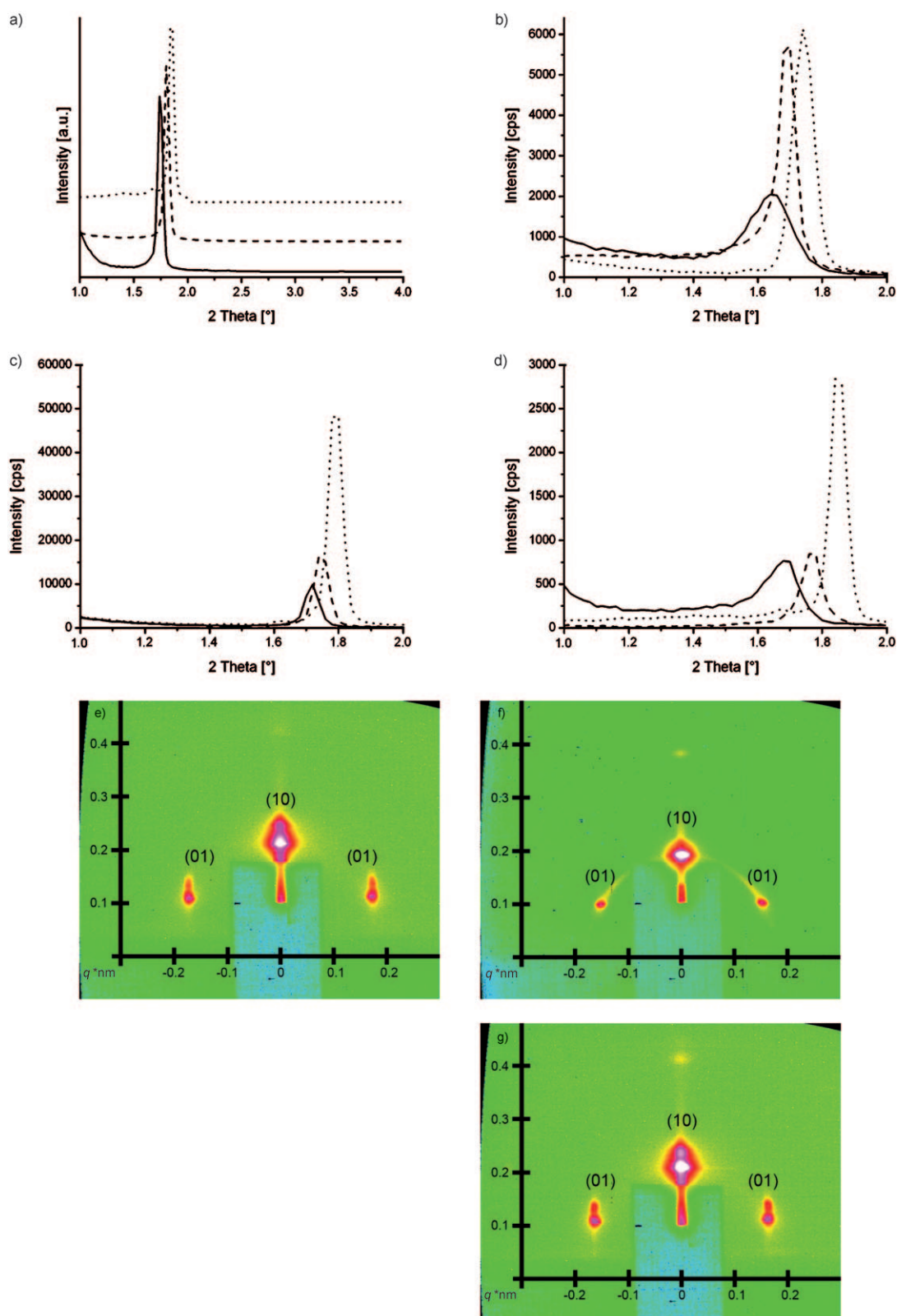


Figure 1. Structural analysis. a–d) 1D X-ray diffractograms of functionalized silica films with varying lengths of alkyl-chains (a; methyl (—), ethyl (---), propyl (·····)); functionalization density 10 mol%, normalized to the reflection with maximum intensity), with varying amounts of cyanopropyl functionalization (b; 5.0 (–), 10 (– · – · –), and 20 mol% (·····)), with varying amounts of phenyl-functionalization (c; 5.0 (–), 10 (– · – · –), and 20 mol% (·····)), and with varying amounts of propyl functionalization (d; 2.5 (—), 5 (---), and 10 mol% (·····)). e–g) GISAXS patterns of 10 mol% propyl-functionalized (e), 20 mol% cyanopropyl-functionalized (f), and 20 mol% phenyl-functionalized (g) silica films. The double peaks in e) and g) arise at very low incident angles when the distorted-wave Born approximation becomes important for highly reflective surfaces.<sup>[29]</sup> At very low angles the incoming beam can be reflected from the substrate and then scattered by the top film, and this leads to the observed shift of Bragg-like peaks to higher angles. The lower the incoming angle the larger the distance between the two reflections.

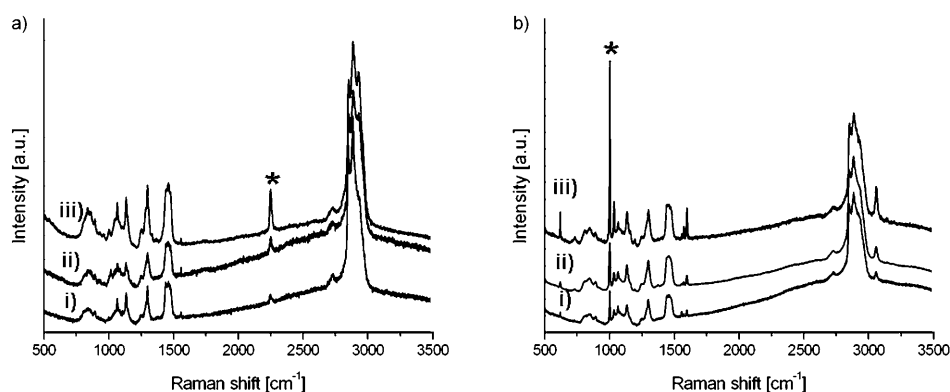


Figure 2. Raman spectra of a) cyanopropyl-functionalized films (functionalization density 5.0 (i), 10 (ii), and 20 mol % (iii)) and b) phenyl-functionalized films (functionalization density 5.0 (i), 10 (ii), and 20 mol % (iii)). The data were normalized to the maximum intensity of the C–H vibration of the template (2886  $\text{cm}^{-1}$ ). The asterisks indicate the signal corresponding to a) the C–N vibration (2236  $\text{cm}^{-1}$ ) and b) the aromatic C–H vibrations of the phenyl group (1000  $\text{cm}^{-1}$ ).

molecules (see Experimental Section) were embedded into the pores of a hexagonal mesoporous thin film at very low concentration ( $10^{-10}$ – $10^{-11}$   $\text{molL}^{-1}$ ) to ensure that they can be observed individually. For single-molecule optical microscopy studies, we use a terrylene diimide derivative due to its high photostability and quantum efficiency.<sup>[22]</sup> As we wish to investigate the influence of the functional groups inside the pores on the diffusion of the dye molecules, we need to ascertain that the molecules are indeed traveling through the pore system and not only on the film surface. This is shown by two different experiments. First, molecules that are on the film surface can be washed off.<sup>[19c]</sup> Each mesoporous film investigated in this study was washed, and the amount of dye molecules visible in the wide-field image was not diminished. This indicates that the molecules are inside the channel system. Second, molecules on the surface move in a two-dimensional random fashion, whereas molecules inside the nanoporous host move along the channels and therefore reflect the structure of the silica matrix.<sup>[19c]</sup> The diffusional motion of the dye inside the mesoporous films is highly structured because it maps the underlying porous network.

To visualize the dynamic behavior of the dye molecules, frame sequences of consecutive wide-field images were recorded. In each individual frame the position of a single molecule is fitted by a two-dimensional Gaussian function [see Eq. (2) in the Supporting Information] from which a trajectory of the molecule as a detailed map of its movements can be obtained. The single molecules can act as reporters that shed light on the nature and quality of the structure in the silica matrix. As was shown previously, it is possible to directly correlate porous structures detected by transmission electron microscopy with the diffusion dynamics of single molecules inside confined porous systems, as detected by optical microscopy.<sup>[19d]</sup>

Figure 4 displays trajectories of single dye molecules in differently functionalized surfactant-containing films. The small black squares indicate the positioning accuracy for each point of the trajectory, which is typically around 15 nm. Molecules 1 and 2 were measured in an ethyl functionalized film. The trajectory of molecule 1 clearly maps a curved domain of three parallel aligned pore systems as well as an area of linearly arranged channels. Unbranched trajectories can also be observed in these films (see molecule 2). Molecules 3 and 4 were recorded in propyl-functionalized films. The trajectories of molecules 3 and 4 indicate a highly structured porous network in the film. Even circularly connected pore systems could be observed (see molecule 4). The trajectories shown in Figure 4 typically span a few micrometers. Similar well-structured trajectories were observed for all film types discussed here and reveal the confined diffusion of the dye molecules in these porous films.

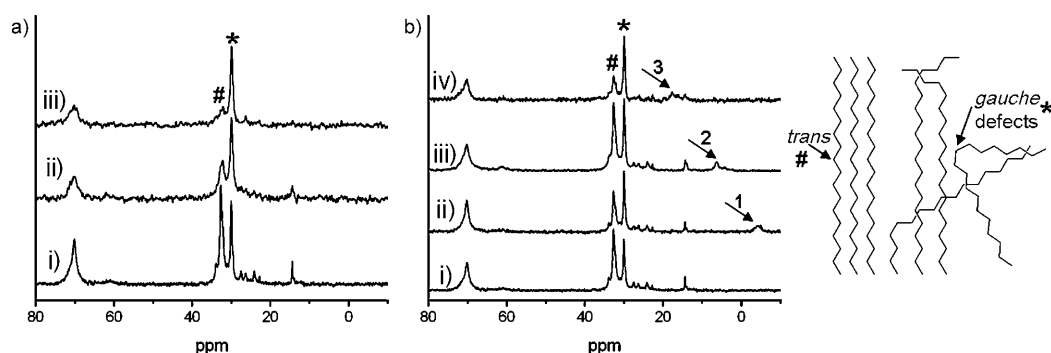


Figure 3.  $^{13}\text{C}$  NMR spectra of a) phenyl-functionalized silica (unfunctionalized (i), 2.5 mol % (ii), 20 mol % (iii)) and b) alkyl-functionalized silica synthesized in anodic alumina membranes (unfunctionalized (i), methyl (ii), ethyl (iii), and propyl (iv); functionalization density 10 mol %, arrows indicate the signal(s) corresponding to the functional group; the numbers above the arrow indicate the number of C atoms in the functional group). The inset shows a graphical illustration of the *gauche* (\*) and *trans* (#) conformations.

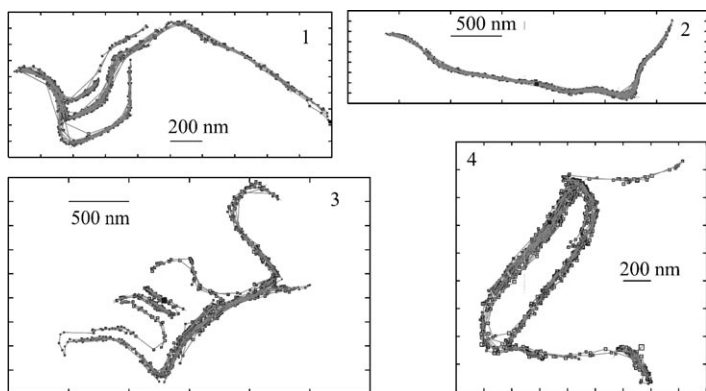


Figure 4. Trajectories of single dye molecules from ethyl- (1 and 2) and propyl-functionalized (3 and 4) films. The functionalization density was 10 mol% and the films were measured at 80% relative humidity. The tiny black squares indicate the positioning accuracy for each point of the trajectory, which is typically around 15 nm.

**Diffusion dynamics in mesoporous films:** The channels of the mesoporous silica thin films contain the template molecules and a certain amount of water, due to the synthesis of the samples by evaporation-induced self-assembly from an ethanol/water solution. It was shown previously that vapor-phase water has a profound effect on the diffusion of Nile Red<sup>[22]</sup> as well as a terylene diimide derivative<sup>[19f]</sup> in silica films. Therefore, a change in the relative humidity at which the samples are measured is also expected to have significant effects on the diffusion of the guest molecules in the functionalized films.

Diffusion of dye molecules in a methyl-functionalized film of 10 mol% functionalization density (a functional group is covalently attached to about every tenth silicon atom) was studied at different relative humidities (30, 50, and 80%; Figure 5). The change in humidity has a profound effect on the mean diffusion coefficient, which increases from 1100 (30) to 3870 nm<sup>2</sup>s<sup>-1</sup> (80%). Additionally, ethyl- and propyl-functionalized films were measured at 30% and 80% relative humidity with 10 mol% functionalization density, and a similar trend of increasing mean diffusion coefficient with increasing humidity was observed. For comparison, the mean diffusion coefficient in an unfunctionalized film is also shown in Figure 5. The detailed data for all films discussed above are summarized in Table 2.

To analyze the water content in the films at different relative humidities, measurements with a quartz-crystal microbalance (QCM) were performed with a propyl-functionalized film. Figure 6 clearly shows that increasing the relative humidity from 30 to 80% leads to an increase in the amount of water adsorbed in the film. This process is fully reversible and reproducible, as can be seen by the three cycles (30→80→30%) shown in the figure. The change in water content from 30 to 80% relative humidity is accompanied by an increase in the mean diffusion coefficient by a factor of 2.8. All mesoporous thin films discussed below were measured at 30% relative humidity in order to analyze the diffusion

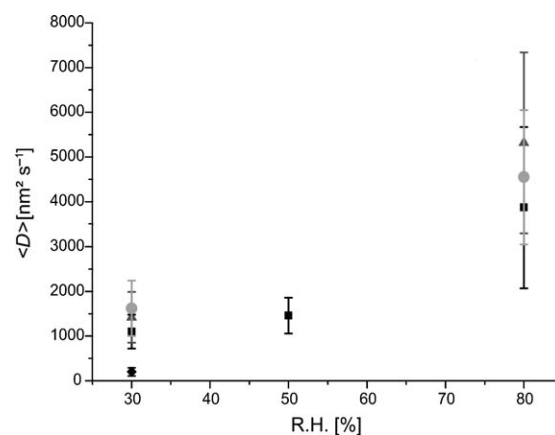


Figure 5. Influence of the surrounding relative humidity (R.H.) on the mean diffusion coefficient of the dye molecules. The data were obtained from methyl- (black squares), ethyl- (dark triangles), and propyl-functionalized (gray circles) films with 10 mol% functionalization density and from an unfunctionalized sample (black rhombus). The bars indicate the width of the distribution of the diffusion coefficients due to the heterogeneity of the samples and not the error in the determination of the mean diffusion coefficients.

Table 2. Diffusion data for measurements at different relative humidities. Functionalization density for the functionalized films: 10 mol%.

Functionalization	None	Methyl		Ethyl		Propyl		
R.H. [%]	30	30	50	80	30	80	30	80
no. of evaluated molecules	101	100	60	80	80	39	104	20
$\langle D \rangle$ [nm <sup>2</sup> s <sup>-1</sup> ]	200	1100	1460	3870	1420	5320	1620	4550
$\sigma$ [nm <sup>2</sup> s <sup>-1</sup> ]	90	380	400	1800	570	2020	620	1500

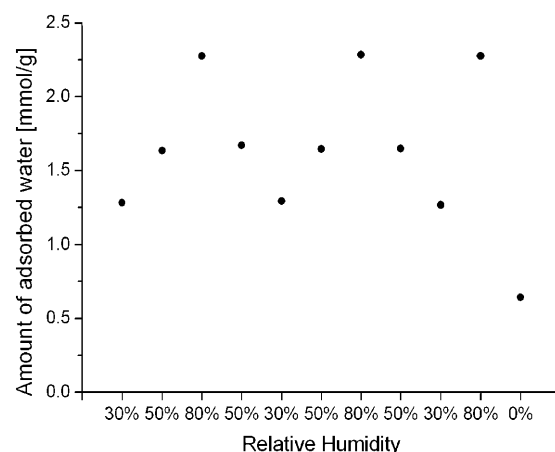


Figure 6. QCM measurements showing the amount of water adsorbed at different relative humidities for a 10 mol% propyl-functionalized silica film. The sample was measured repeatedly between 30 and 80% relative humidity.

coefficients of the dye molecules under comparable conditions.

In the following we examine the influence of functionalization density on the diffusion coefficient of the DIP-TDI



dye, which can be extracted from the trajectories (see Supporting Information). Figure 7a compares three cyanopropyl-functionalized films, with functionalization densities of 5.0, 10, and 20 mol%. In each of the films at least 80 molecules were measured and analyzed. The diffusion coefficients of all analyzed molecules were determined and then plotted as histograms. The histograms reveal the individual dynamics of the single molecules traveling through the system. They are quite broad and reflect the heterogeneity of the sample. The mean diffusion coefficient, shown in Figure 7d, increases substantially with increasing functionalization density, from  $410 \text{ nm}^2 \text{ s}^{-1}$  (5.0 mol%) to  $2820 \text{ nm}^2 \text{ s}^{-1}$  (20 mol%). This corresponds to an increase by a factor of about seven.

In Figure 7b, the diffusion coefficients of propyl-functionalized samples of 2.5, 5.0, and 10.0 mol% functionalization density are displayed as histograms. Again, the mean diffusion coefficient changes significantly with functionalization

density, from  $380 \text{ nm}^2 \text{ s}^{-1}$  (2.5 mol%) to  $1620 \text{ nm}^2 \text{ s}^{-1}$  (10 mol%). This corresponds to a fourfold increase.

Figure 7c shows histograms of diffusion coefficients for different phenyl-functionalization densities between 2.5 and 30 mol%. For this functionality the film structure is retained even for high densities. In contrast to the above samples functionalized with flexible chains (Figure 7a and b), here the mean diffusion coefficient decreases with increasing functionalization density. The dye inside the film is slowed down by nearly one order of magnitude from a diffusion coefficient of  $650 \text{ nm}^2 \text{ s}^{-1}$  (2.5 mol%) to  $80 \text{ nm}^2 \text{ s}^{-1}$  (30 mol%).

Figure 7d visualizes the different trends discussed above. Additionally, the mean diffusion coefficient for the unfunctionalized film is given ( $200 \text{ nm}^2 \text{ s}^{-1}$ ). The bar for each data point does not indicate the error in the determination of the mean diffusion coefficient. It rather indicates the width of the distribution of the diffusion coefficients due to the heterogeneity of the samples.

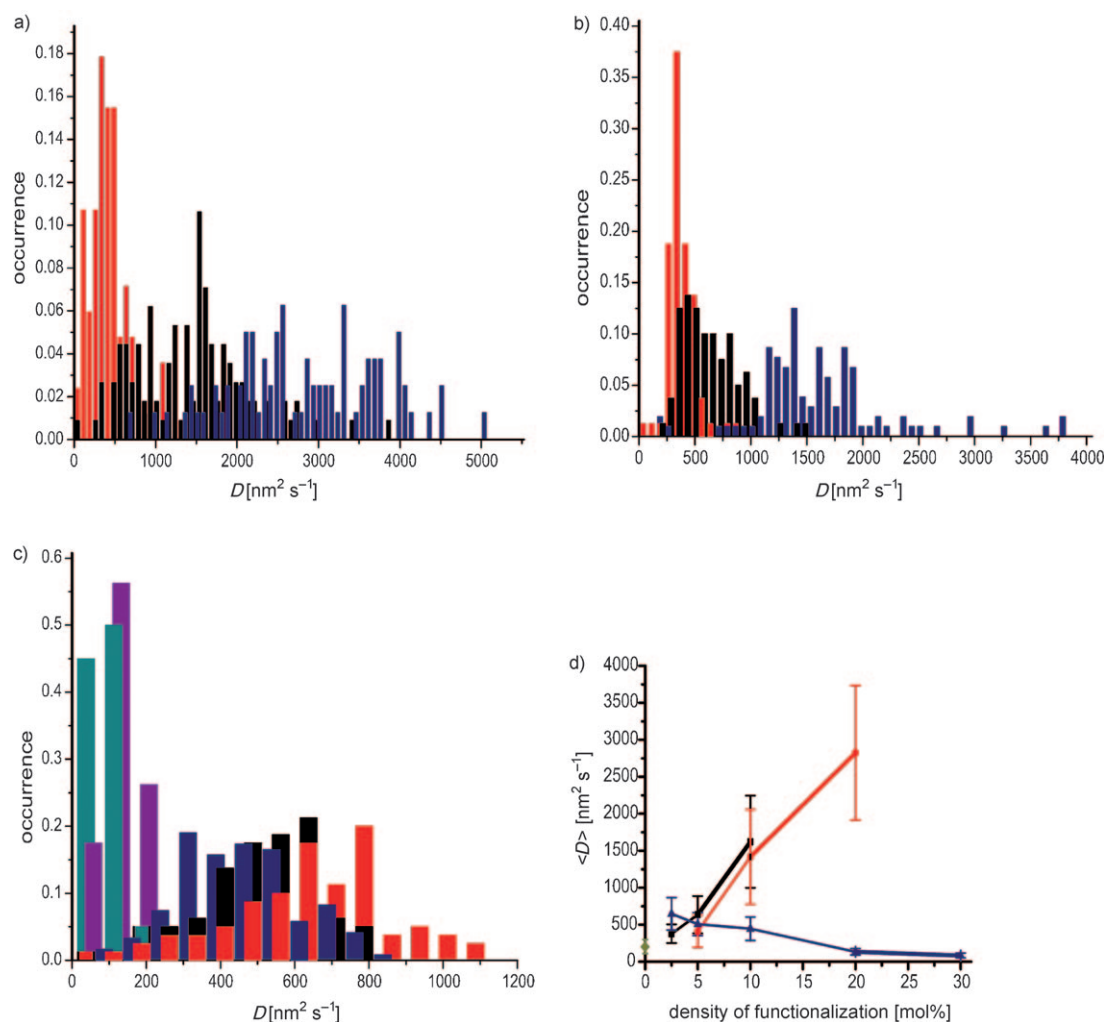


Figure 7. Diffusion data for the functionalization density experiments (measured at 30% relative humidity). Histogram for a) different cyanopropyl functionalization densities, plotted in different colors (red: 5.0, black: 10, blue: 20 mol%); b) varying propyl functionalization densities (red: 2.5, black: 5.0, blue: 10 mol%); and c) a series of different phenyl functionalization densities (red: 2.5, black: 5.0, blue: 10, purple: 20, light blue: 30 mol%). d) Correlation of the mean diffusion coefficients with the functionalization densities, including the data for the unfunctionalized film, given at zero density (black: propyl, red: cyanopropyl, blue: phenyl, green: unfunctionalized). The bars indicate the width of the distribution of the diffusion coefficients due to the heterogeneity of the samples and not the error in the determination of the mean diffusion coefficients.

ogeneity of the samples. The distributions were calculated by fitting the experimental data to a 1D Gaussian function.

The nature of the functional groups was also changed in order to explore their influence on guest dynamics (Figure 8). The template-containing films discussed in this section were synthesized with 10 mol% functionalization density. In Figure 8a, the diffusion data for aliphatic functional groups with different alkyl chain lengths (methyl, ethyl, and propyl) are shown. The change in diffusion coefficients due to different alkyl groups (Figure 8a) is less significant than the change due to different functionalization densities, for example, propyl densities (see Figure 7a). However, an increase in diffusivity can be observed for increasing alkyl chain lengths; the diffusion coefficient increases from 1100 to 1620 nm<sup>2</sup>s<sup>-1</sup> (from methyl to propyl functionality). Samples with longer aliphatic chains were also prepared (pentyl and octyl functionalization). However, it was not possible to acquire reproducible data as the structural definition of these films was insufficient.

Figure 8b displays the influence of functional-group polarity on the diffusion coefficients by comparing propyl-, cyanopropyl-, and trifluoropropyl-functionalized films. The strongly polar trifluoropropyl groups decrease the mean diffusion coefficient of the dye to about one-half (740 nm<sup>2</sup>s<sup>-1</sup>) of those of the propyl- and cyanopropyl-functionalized films (1620 nm<sup>2</sup>s<sup>-1</sup> and 1420 nm<sup>2</sup>s<sup>-1</sup>). Thus, increasing polarity of the functional groups leads to a decrease in dye dynamics.

The complete data obtained from these measurements are summarized in Table 3.

**Correlation of the diffusion coefficients to the pore-to-pore distance:** The question arises whether the changes in the pore-to-pore distances observed for different functionalization densities (Figure 1 and Table 1) are correlated with the dynamics of the molecules. Therefore, we plotted the mean diffusion coefficients evaluated from the data of Figure 7 to pore-to-pore distances obtained from 1D X-ray diffraction (Figure 9). In the propyl- and cyanopropyl-functionalized samples, an increase of the mean diffusion coefficient can be observed for decreasing pore-to-pore distance. In contrast, in phenyl-functionalized films a decreasing pore-to-pore distance correlates with a decrease in dye dynamics. From this we can conclude that the effect on the mobility of the dye discussed for the data in Figure 7 cannot be due to a simple change in the pore-to-pore distance. The underlying mechanisms that govern dye dynamics in the presence of functional groups appear to be more complex and will be discussed later.

Table 3. Diffusion data for measurements at a relative humidity of 30%.

Functionalization	None	Methyl	Ethyl	Propyl					
functionalization density [mol%]	–	10	10	2.5	5.0	10			
no. of evaluated molecules	101	100	80	80	80	104			
D  [nm <sup>2</sup> s <sup>-1</sup> ]	200	1100	1420	380	640	1620			
σ [nm <sup>2</sup> s <sup>-1</sup> ]	90	380	570	130	250	620			
Functionalization	Cyanopropyl			Phenyl			Trifluoropropyl		
Functionalization density [mol%]	5.0	10	20	2.5	5.0	10	30	10	
no. of evaluated molecules	84	113	80	80	80	121	80	80	100
D  [nm <sup>2</sup> s <sup>-1</sup> ]	410	1420	2820	650	510	450	130	80	740
σ [nm <sup>2</sup> s <sup>-1</sup> ]	220	640	910	220	160	160	40	30	280

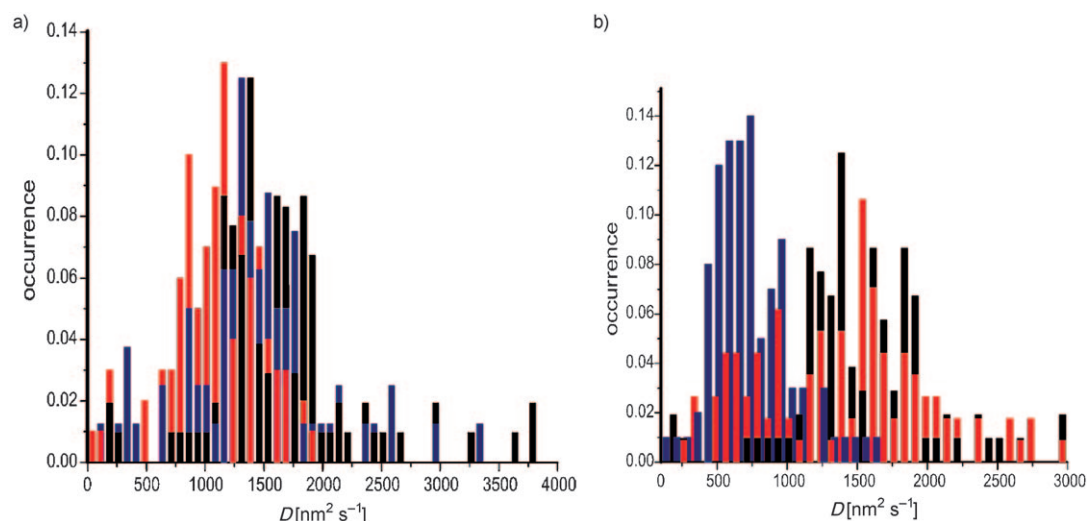


Figure 8. Influence of the a) alkyl chain length (red: methyl, blue: ethyl, black: propyl) and b) the polarity of the functional groups (red: cyanopropyl, blue: trifluoropropyl, black: propyl) on the diffusion dynamics of the guest molecules. The films in a) and b) were synthesized with 10 mol% functionalization density and measured at 30% relative humidity.

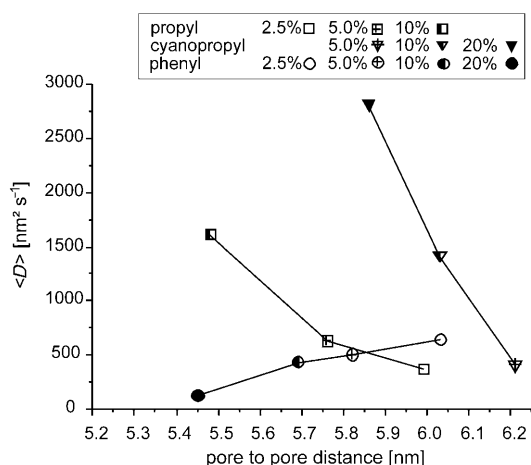


Figure 9. Correlation of the diffusion coefficients for the different functionalization densities with the pore-to-pore distances from 1D X-ray diffraction measurements. Data of propyl-functionalized films are displayed as squares, data from cyanopropyl-functionalized films as triangles, and data of phenyl-functionalized samples as circles.

**Heterogeneities:** The above results show that we can strongly influence the diffusion dynamics of guest molecules by the introduction of functional groups. We now ask whether the functional groups are homogeneously distributed inside the porous network. The behavior of single molecules can offer unique insights into these structural details of the pore system. Inhomogeneities in the distribution of functional groups are local variations in the functionalization density. As we know from Figure 7, these variations lead to very pronounced effects on the diffusion dynamics of the guest molecule. Cyanopropyl-functionalized films (20 mol % func-

tionalization density) are ideally suited for detecting heterogeneities through the diffusional behavior of the embedded dye molecules, because the dyes respond strongly to variations in the functionalization density in these films (see Table 3).

While we previously mentioned the heterogeneity from molecule to molecule in the mesoporous films, we now focus on possible heterogeneities within a single molecule trajectory. For this purpose, Figure 10a displays the results of a more detailed analysis of the ranked step length distribution (see Supporting Information) by plotting the inverse of the cumulative probability of the squared step lengths for a single dye molecule. We used this method previously to characterize inhomogeneities of single molecule diffusion in unfunctionalized mesoporous silica films.<sup>[19c]</sup> The data points display the step lengths according to their rank. The green line indicates a mono-exponential fit, and the blue line a bi-exponential fit. Clearly the mono- and bi-exponential functions are not sufficient to fit the data adequately. This indicates that the diffusion of the dye molecule is extremely heterogeneous and cannot be described by only one or two diffusion coefficients. Similar data can be obtained for any other functionalization as well as for unfunctionalized films.

Further, we ask whether these contributions of different diffusion coefficients for a single molecule can be assigned to local variations in the functional-group density within different branches of the trajectory. For this purpose, we display the trajectory such that the different classes of step lengths (short, medium, and long steps) are displayed in different colors. As each wide-field image in the whole frame sequence is recorded with the same integration time, longer steps are more likely associated with a higher local diffusion

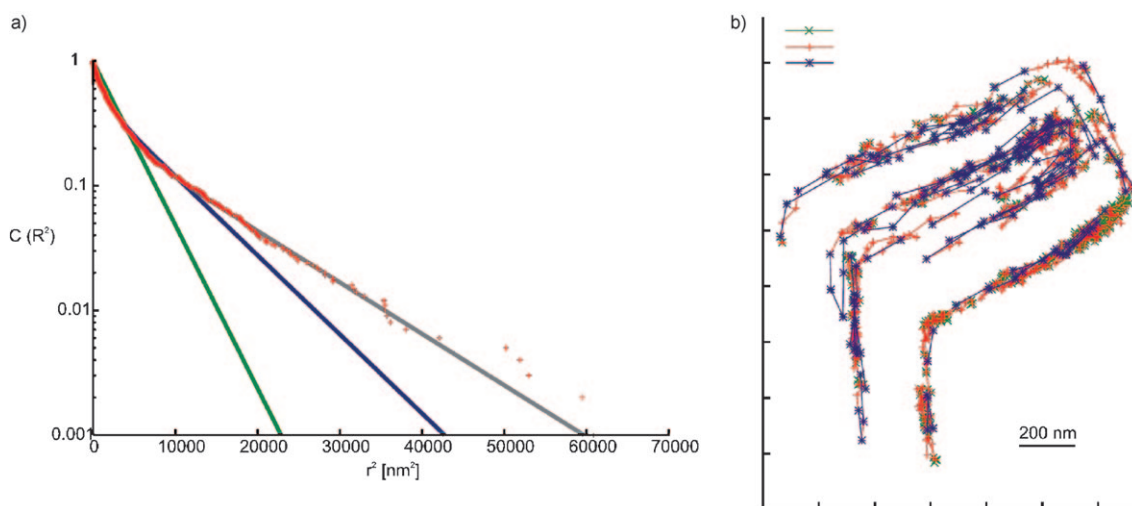


Figure 10. Exemplary data of one molecule diffusing in a 20 mol% cyanopropyl-functionalized film. a) The ranked step length distribution is shown by plotting the inverse of the cumulative probability distribution for  $t_{\text{lag}} = \tau$  [see Eq. (6) in Supporting Information]. The green line shows a mono-exponential, the blue line a bi-exponential, and the gray line a tri-exponential fit. The fitting parameters according to Equation (7) in the Supporting Information for a mono-exponential decay are:  $c_1 = 1.000$  and  $r_1^2 = 3316 \text{ nm}^2$ . The bi-exponential fit gives the following parameters:  $c_1 = 0.479$ ,  $r_1^2 = 907 \text{ nm}^2$ ,  $c_2 = 0.521$ ,  $r_2^2 = 6621 \text{ nm}^2$ . The tri-exponential fit gives the following parameters:  $c_1 = 0.149$ ,  $r_1^2 = 164 \text{ nm}^2$ ,  $c_2 = 0.557$ ,  $r_2^2 = 2006 \text{ nm}^2$ ,  $c_3 = 0.294$ ,  $r_3^2 = 10301 \text{ nm}^2$ . To fit the data (red crosses) adequately a tri-exponential fit is needed; this illustrates the inherent heterogeneity of the template-containing film. b) Trajectory of the molecule; the step lengths are grouped into three classes and plotted in different colors (short steps (green)  $\leq 27 \text{ nm}$ , medium steps (red)  $27\text{--}100 \text{ nm}$ , long steps (blue)  $\geq 100 \text{ nm}$ ).



coefficient. Figure 10b shows this analysis for the same molecule shown in Figure 10a. Through variation of the threshold values for the different step lengths, local heterogeneities in the diffusion coefficient caused by the functional-group density of different branches in the same trajectory should become apparent. They would be visualized as local accumulations of steps of the same class of length. However, the different step lengths are statistically distributed over the trajectory. Therefore no spatial correlation between the distinct values of  $D$  observed in Figure 10a and specific areas of the molecular trajectory (Figure 10b) can be detected. Thus, the heterogeneities revealed by the plot in Figure 10a must lie below our limits of spatial resolution.

The lower limit to which we can visualize local density fluctuations for the functional groups depends on the diffusion coefficient of the single molecule and can be roughly estimated as follows: The dye molecules in the sample evaluated in Figure 10 show a mean diffusion coefficient of  $2820 \text{ nm}^2 \text{ s}^{-1}$ . A single wide-field frame in the whole sequence was recorded with an integration time of 400 ms. During this time the dye molecules explore an average distance of  $\sqrt{|r^2|}$  [see Eq. (2)] of about 67 nm.

## Discussion

Our experiments confirm that the surrounding relative humidity has a profound influence on the diffusion of dye molecules inside functionalized mesoporous films. For all samples studied, we observed that with increasing relative humidity the dye molecules move faster in the host material (see Table 2). From QCM measurements we know that increasing the relative humidity of the environment surrounding the film leads to detectable increases in the amount of water adsorbed (see Figure 6). The silica pore walls are covered with hydroxyl groups (for unfunctionalized silica it is estimated that there are around four hydroxyl groups per square nanometer).<sup>[23]</sup> They can interact with the oxygen atoms of the dye by forming hydrogen bonds. As was previously reported,<sup>[19e,f]</sup> this leads to a decrease in the dynamics of the dye due to adsorption sites. We therefore suggest that the accessibility of these surface hydroxyl groups has a significant influence on the diffusion dynamics of the dye molecule. If we assume that an average silica film has a surface area of  $800 \text{ m}^2 \text{ g}^{-1}$  (a typical value for these mesoporous materials),<sup>[24]</sup> we can estimate the coverage of water molecules on the silica surface at different relative humidities. For the 10 mol% propyl-functionalized film, the coverage of water molecules at 30% relative humidity is then calculated to be about one water molecule per square nanometer. At 80% relative humidity the coverage is about 1.7 water molecules per square nanometer. At higher relative humidity, the adsorbed water will therefore have a greater shielding effect on the hydroxyl groups, leading to faster diffusion dynamics, as observed in this study.

Our experiments further show that variations in water content alone do not explain the observed changes in diffu-

sion dynamics of dye molecules in differently functionalized films. According to QCM measurements, the unfunctionalized film contains a much larger amount of water than the propyl-functionalized film. However, a lower mean diffusion coefficient is obtained from the measurements in an unfunctionalized film compared to propyl-functionalized films at 30% relative humidity (see Table 3). As discussed above, hydrogen bonds between the oxygen atoms of the dye and surface hydroxyl groups have an important influence on dye dynamics. The introduction of flexible alkyl groups reduces the number of hydroxyl groups on the surface of the pores and can result in shielding of the remaining hydroxyl groups. This reduces the accessible sites for hydrogen bonding and thereby allows the dye to diffuse faster. The shielding effect of water is less pronounced than that of apolar alkyl chains, as there is no possibility of hydrogen bonding between the functional group and the dye molecule. The shielding of hydroxyl groups also explains the increase in the mean diffusion coefficient with increasing alkyl chain length described in Figure 8a, as longer chains can be assumed to have a greater shielding effect. Similarly, the effects observed for increasing propyl and cyanopropyl functionalization densities (Figure 7a and b) can be explained. Furthermore, cyanopropyl groups can have a similar shielding effect to that described for propyl groups. Consequently, faster diffusion is observed in cyanopropyl-functionalized compared to unfunctionalized films (Figure 7d). Due to our synthesis conditions the solution inside the pores is acidic and results in protonation of the cyano groups. Hence, weak hydrogen bonds can form between the dye and the functional groups. This explains our observation that the mean diffusion coefficient in cyanopropyl-functionalized films is lower than in propyl-functionalized films (Figure 7d). The effect observed for trifluoropropyl functionalization (Figure 8b) may similarly be attributed to the polarity. However, additional effects, such as wetting, may also play a role.

The effects observed for phenyl functionalization can be explained by two competing processes. For low functionalization densities (2.5 and 5.0 mol%) the shielding effect discussed above results in a higher mean diffusion coefficient compared to the unfunctionalized film (Figure 7d). At the lowest functionalization density the bulky and rigid phenyl groups show the best shielding effect of all functional groups studied. Consequently, at this density the largest mean diffusion coefficient was obtained in phenyl-functionalized films. Interestingly, the mean diffusion coefficient decreases with increasing functionalization density for phenyl-functionalized films (Figure 7c). According to the proportions displayed in Figure 11, which is drawn to scale, it is reasonable to assume that the observed effects can be partially due to direct interaction of the dye with the functional groups. The decreasing mean diffusion coefficient with increasing functionalization density can therefore be explained by attractive  $\pi$ - $\pi$  interactions between the rigid phenyl groups and the aromatic system of the dye or the phenyl groups at both ends of the dye. Due to the diisopropyl groups in the dye, these end groups are twisted out of the

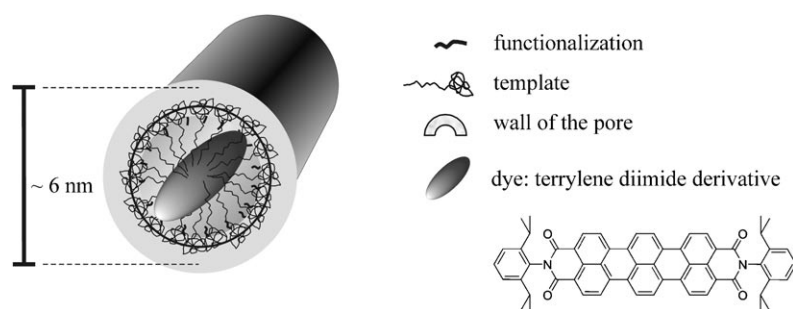


Figure 11. Sketch of a DIP-TDI dye molecule within one pore. All constituents are drawn to scale. The chemical structure of the dye is displayed on the right.

aromatic plane of the dye. This is sterically advantageous for interactions with the phenyl functionality.

An additional factor that can influence the dynamics of the dye molecule is the rigidity of the template micelles. According to NMR data the degree of disorder of the alkyl chains of the template molecules depends on the functional groups and their density (Figure 3). We suggest that the micelle packing is less rigid when the alkyl chains of the template molecules are less ordered, that is, show a larger number of gauche defects. Therefore, the dye molecules can more easily pass through the template-containing film. With increasing length of the alkyl functional groups, the degree of disorder increases. Accordingly, the mean diffusion coefficient of the dye molecules is larger for longer chain alkyl functionalization (Figure 8a). This also explains the observation that at a low density (5.0 mol%) the mean diffusion coefficient observed in a phenyl-functionalized film is larger than in films with other functionalization, because already at 2.5 mol% phenyl functionalization the degree of disorder of the alkyl chains of the template molecules is greater than in the 10 mol% alkyl-functionalized samples. Again, this can be deduced from the significantly smaller ratio of *trans* to *gauche* signal in the phenyl-functionalized sample. However, while the degree of disorder in the template micelles in a film with 20 mol% phenyl functionalization is greater than that of the 2.5 mol% functionalized sample, we do not observe an increase in the mean diffusion coefficient. This suggests that at this high functionalization density direct  $\pi$ - $\pi$  interactions between the functional groups and the dye have a greater influence on the dye dynamics than the order and rigidity of the micelle packing.

To summarize, the changes in the mean diffusion coefficient of a dye molecule moving through a functionalized mesoporous silica film can be explained by considering the shielding of silanol groups in combination with changes in the rigidity of the micelle packing of the template in the film and direct interactions between the functional groups and the dye molecules.

## Conclusion

We have shown that the incorporation of functional groups has a profound influence on the diffusional behavior of dye molecules inside surfactant-containing mesoporous silica films. The advanced microscopy techniques employed here are uniquely suited to revealing the mechanistic details of the host-guest interactions at the single-molecule level. Molecular diffusion

is heterogeneous both in space and time. Furthermore, this comprehensive study illustrates that functional groups can be used to slow down or accelerate the diffusion of guest molecules over one order of magnitude. This opens up the opportunity to fine-tune host-guest interactions in these systems. For example, such interactions are of great interest when mesoporous hosts are used as drug-delivery systems, for which controlling the drug release rate is of paramount importance. Thus, a deceleration in guest dynamics, as observed for the phenyl-functionalized samples, can generate a depot effect, that is, the incorporated drug will be slowly released over a prolonged period of time.

## Experimental Section

**Synthesis of DIP-TDI/mesoporous system:** The functionalized mesoporous silica films were synthesized by the evaporation-induced self-assembly (EISA) method.<sup>[25]</sup> Samples were prepared by spin coating precursor solutions onto cleaned glass cover slips. For the preparation of precursor solutions for unfunctionalized films, tetraethoxysilane (TEOS, 10 mmol, 2.08 g) in ethanol (3.83 g) was prehydrolyzed at 60 °C for 1 h with acidic catalysis (3 g of 0.2 M hydrochloric acid and 1.8 g of water). The Brij-56 structure-directing agent (566 mg) in ethanol (7.81 g) was added. *N,N'*-Di(2,6-diisopropylphenyl)terrylene-3,4:11,12-tetracarboxydiimide (DIP-TDI),<sup>[26]</sup> a very photostable dye with a high fluorescence quantum yield (Figure 11), was added to the solution at an ultralow concentration ( $10^{-10}$ – $10^{-11}$  mol L<sup>-1</sup>). Then 80  $\mu$ L of this precursor solution was spin coated at 3000 rpm for 1 min onto a cover slip to give a structured silica film on the glass surface. For the synthesis of the functionalized silica films, a certain molar fraction (2.5, 5, 10, 20, or 30 mol%) of the silica source (TEOS) was replaced with a functionalized silica source (Table 4). The other reaction conditions were kept constant.

**X-ray diffractometry (XRD):** The structure of the pores in the film was determined by using a Scintag XDS 2000 powder diffractometer in  $\theta/\theta$  Bragg-Brentano scattering geometry.

**Grazing-incidence small-angle X-ray scattering (GISAXS):** Experiments were performed at beamline BL 5.2 L of the electron storage ring ELETTRA (Triest, Italy). The wavelength of the incident beam was 0.155 nm (8 keV), and the sample-detector distance 640 mm. The data were recorded in reflection geometry close to the total-reflection angle to achieve maximum intensity.

**Raman and solid-state nuclear magnetic resonance (NMR) spectroscopy:** As the volume of the thin films is very small, we utilized a model system providing a larger sample volume to access a wider spectrum of analytical techniques and to achieve an optimal signal-to-noise ratio for the analysis of functionalized mesoporous silica synthesized by the EISA method (see Supporting Information for details). Raman spectra of these samples

Table 4. Silica sources used to incorporate the respective functionalizations.

Functionalization	Silica source
methlyl	CH <sub>3</sub> Si(OC <sub>2</sub> H <sub>5</sub> ) <sub>3</sub>
ethyl	C <sub>2</sub> H <sub>5</sub> Si(OCH <sub>3</sub> ) <sub>3</sub>
propyl	C <sub>3</sub> H <sub>7</sub> Si(OCH <sub>3</sub> ) <sub>3</sub>
cyanopropyl	CNC <sub>3</sub> H <sub>6</sub> Si(OC <sub>2</sub> H <sub>5</sub> ) <sub>3</sub>
phenyl	C <sub>6</sub> H <sub>5</sub> Si(OC <sub>2</sub> H <sub>5</sub> ) <sub>3</sub>
trifluoropropyl	F <sub>3</sub> C <sub>3</sub> H <sub>4</sub> Si(OCH <sub>3</sub> ) <sub>3</sub>

were recorded on a Horiba Jobin Yvon HR800 UV Raman microscope by using an He–Ne laser emitting at 633 nm. Solid-state <sup>13</sup>C NMR measurements in cross-polarization mode were performed on a Bruker DSX Advance 500 FT (contact time 2 ms, spinning rate 6.0 kHz, pulse delay 2.8 μs, recycle delay 8 s, number of scans between 640 and 16400).

**Quartz-crystal microbalance (QCM):** The quartz crystal microbalance (QCM) technique is based on the fact that the frequency of an oscillating QCM is proportional to the additional adsorbed mass.<sup>[27]</sup> Provided the porous material can be deposited as an acoustically coupled thin film on the surface of the device, one can measure the uptake of adsorbed material on the nanogram scale as a function of partial pressure and temperature via the frequency changes of the QCM. Here, the amount of water adsorbed in the silica films was measured with a QCM experimental setup that was previously described in detail (see also Supporting Information).<sup>[28]</sup>

**Wide-field microscopy and single-particle tracking:** Fluorescence images were recorded with a wide-field setup on an Eclipse TE200 (Nikon) epifluorescence microscope with a high numerical aperture oil-immersion objective (Nikon Plan Apo 100×/1.40 N.A. oil). The molecules were excited at 633 nm with a He–Ne gas laser with an intensity of 0.20 kWcm<sup>-2</sup>, and their fluorescence was detected with a back-illuminated electron-multiplying charge-coupled device (EM-CCD) camera in frame-transfer mode (Andor iXon DV897, 512×512 pixels). Incident laser light was blocked by a dichroic mirror (640 nm cutoff, AHF) and a bandpass filter (730/140, AHF). Details of the setup were reported previously.<sup>[19c]</sup> The obtained data were analyzed as described in the Supporting Information.

To record wide-field movies of differently humidified samples, a sample chamber was mounted around the samples in which chamber the relative humidity was adjusted by mixing a dry stream of pressurized air with a humidified stream. The samples were stored under the resulting humidity for 10 min before the measurement started. This time proved to be sufficient for equilibration.

**Ranked step length distribution:** Analysis of the distribution of ranked step lengths offers more detailed insight into the motional behavior of the single particles. It allows one to extract several diffusion coefficients contained in the recorded movement of the molecule in case of heterogeneities. The method is described in detail in the Supporting Information.

## Acknowledgements

We thank C. Minke from the Department of Chemistry and Biochemistry, University of Munich, for the solid-state NMR measurements. We further thank B. Platschek and T. Reuther from the Department of Chemistry and Biochemistry, University of Munich, for support with the QCM measurements. For support with the GISAXS measurements, we thank A. Keilbach and A. Zürner from the Department of Chemistry and Biochemistry, University of Munich. Financial support from the Nanosystems Initiative Munich (NIM) and the SFBs 486 and 749 (all DFG) is gratefully acknowledged.

[1] J. S. Beck, J. C. Vartuli, W. J. Roth, M. E. Leonowicz, C. T. Kresge, K. D. Schmitt, C. T. W. Chu, D. H. Olson, E. W. Sheppard, S. B.

- McCullen, J. B. Higgins, J. L. Schlenker, *J. Am. Chem. Soc.* **1992**, *114*, 10834–10843.
- [2] D. E. De Vos, M. Dams, B. F. Sels, P. A. Jacobs, *Chem. Rev.* **2002**, *102*, 3615–3640.
- [3] S. J. L. Billinge, E. J. McKimmy, M. Shatnawi, H. Kim, V. Petkov, D. Wermeille, T. J. Pinnavaia, *J. Am. Chem. Soc.* **2005**, *127*, 8492–8498.
- [4] V. Rebbin, R. Schmidt, M. Fröba, *Angew. Chem.* **2006**, *118*, 5335–5339; *Angew. Chem. Int. Ed.* **2006**, *45*, 5210–5214.
- [5] a) N. Petkov, N. Stock, T. Bein, *J. Phys. Chem. B* **2005**, *109*, 10737–10743; b) B. Ye, M. L. Trudeau, D. M. Antonelli, *Adv. Mater.* **2001**, *13*, 561–565; c) D. J. Cott, N. Petkov, M. A. Morris, B. Platschek, T. Bein, J. D. Holmes, *J. Am. Chem. Soc.* **2006**, *128*, 3920–3921.
- [6] a) C.-Y. Lai, B. G. Trewyn, D. M. Jeftinija, K. Jeftinija, S. Xu, S. Jeftinija, V. S. Y. Lin, *J. Am. Chem. Soc.* **2003**, *125*, 4451–4459; b) I. Roy, T. Y. Ohulchanskyy, D. J. Bharali, H. E. Pudavar, R. A. Mistretta, N. Kaur, P. N. Prasad, *Proc. Natl. Acad. Sci. USA* **2005**, *102*, 279–284; c) S. Giri, B. G. Trewyn, M. P. Stellmaker, V. S. Y. Lin, *Angew. Chem.* **2005**, *117*, 5166–5172; *Angew. Chem. Int. Ed.* **2005**, *44*, 5038–5044; d) F. Torney, B. G. Trewyn, V. S. Y. Lin, K. Wang, *Nanotechnol.* **2007**, *2*, 295–300.
- [7] a) B. Munoz, A. Ramila, J. Perez-Pariente, I. Diaz, M. Vallet-Regí, *Chem. Mater.* **2003**, *15*, 500–503; b) M. Vallet-Regí, F. Balas, D. Arcos, *Angew. Chem.* **2007**, *119*, 7692–7703; *Angew. Chem. Int. Ed.* **2007**, *46*, 7548–7558; c) S. Shen, P. S. Chow, F. Chen, R. B. H. Tan, *Chem. Pharm. Bull.* **2007**, *55*, 985–991; d) S. Giri, B. G. Trewyn, V. S. Y. Lin, *Nanomedicine* **2007**, *2*, 99–111.
- [8] a) H. Provendier, C. C. Santini, J. M. Basset, L. Carmona, *Eur. J. Inorg. Chem.* **2003**, 2139–2144; b) P. M. Visintin, R. G. Carbonell, C. K. Schauer, J. M. DeSimone, *Langmuir* **2005**, *21*, 4816–4823.
- [9] a) T. Maschmeyer, F. Rey, G. Sankar, J. M. Thomas, *Nature* **1995**, *378*, 159–162; b) T. Yokoi, H. Yoshitake, T. Tatsumi, *J. Mater. Chem.* **2004**, *14*, 951–957.
- [10] a) K. Yamamoto, T. Tatsumi, *Chem. Lett.* **2000**, 624–625; b) K. Yamamoto, T. Tatsumi, *Microporous Mesoporous Mater.* **2001**, *44*, 459–464; c) S. Angloher, T. Bein, *J. Mater. Chem.* **2006**, *16*, 3629–3634; d) S. Angloher, J. Kecht, T. Bein, *Chem. Mater.* **2007**, *19*, 3568–3574.
- [11] a) C. E. Fowler, S. L. Burkett, S. Mann, *Chem. Commun.* **1997**, 1769–1770; b) J. Aguado, J. M. Arsuaga, A. Arencibia, *Ind. Eng. Chem.* **2005**, *44*, 3665–3671.
- [12] a) Q. Yang, J. Yang, J. Liu, Y. Li, C. Li, *Chem. Mater.* **2005**, *17*, 3019–3024; b) W. S. Han, Y. Kang, S. J. Lee, H. Lee, Y. Do, Y.-A. Lee, J. H. Jung, *J. Phys. Chem. B* **2005**, *109*, 20661–20664.
- [13] V. Kukla, J. Kornatowski, D. Demuth, I. Girnus, H. Pfeifer, L. V. C. Rees, S. Schunk, K. K. Unger, J. Kärger, *Science* **1996**, *272*, 702–704.
- [14] N. E. Benes, H. Jobic, H. Verweij, *Microporous Mesoporous Mater.* **2001**, *43*, 147–152.
- [15] R. Rigler, U. Mets, J. Widengren, P. Kask, *Eur. Biophys. J.* **1993**, *22*, 169–175.
- [16] M. J. Wirth, D. J. Swinton, M. D. Ludes, *J. Phys. Chem. B* **2003**, *107*, 6258–6268.
- [17] K. Bacia, S. A. Kim, P. Schuille, *Nat. Methods* **2006**, *3*, 83–89.
- [18] Y. Fu, F. M. Ye, W. G. Sanders, M. M. Collinson, D. A. Higgins, *J. Phys. Chem. B* **2006**, *110*, 9164–9170.
- [19] a) C. Hellriegel, J. Kirstein, C. Bräuchle, *New J. Phys.* **2005**, *7*, 23–36; b) C. Jung, C. Hellriegel, J. Michaelis, C. Bräuchle, *Adv. Mater.* **2007**, *19*, 956–960; c) J. Kirstein, B. Platschek, C. Jung, R. Brown, T. Bein, C. Bräuchle, *Nat. Mater.* **2007**, *6*, 303–310; d) A. Zürner, J. Kirstein, M. Dobliger, C. Bräuchle, T. Bein, *Nature* **2007**, *450*, 705–708; e) C. Jung, C. Hellriegel, B. Platschek, D. Wöhrle, T. Bein, J. Michaelis, C. Bräuchle, *J. Am. Chem. Soc.* **2007**, *129*, 5570–5579; f) C. Jung, J. Kirstein, B. Platschek, T. Bein, M. Budde, I. Frank, K. Müllen, J. Michaelis, C. Bräuchle, *J. Am. Chem. Soc.* **2008**, *130*, 1638–1648.
- [20] M. Klotz, P.-A. Albouy, A. Ayrat, C. Menager, D. Grosso, A. van der Lee, V. Cabuil, F. Babonneau, C. Guizard, *Chem. Mater.* **2000**, *12*, 1721–1728.
- [21] V. R. Karra, I. L. Moudrakovski, A. Sayari, *J. Porous Mater.* **1996**, *3*, 77–82.

- [22] C. Jung, B. K. Muller, D. C. Lamb, F. Nolde, K. Mullen, C. Bräuchle, *J. Am. Chem. Soc.* **2006**, *128*, 5283–5291.
- [23] C. J. Brinker, G. W. Scherer, *Sol-Gel Science: The Physics and Chemistry of Sol-Gel Processing*, Academic Press, San Diego, **1990**, p. 620–628.
- [24] Y. Lu, R. Ganguli, C. A. Drewien, M. T. Anderson, C. J. Brinker, W. Gong, Y. Guo, H. Soyez, B. Dunn, M. H. Huang, J. I. Zink, *Nature* **1997**, *389*, 364–368.
- [25] C. J. Brinker, Y. F. Lu, A. Sellinger, H. Y. Fan, *Adv. Mater.* **1999**, *11*, 579–585.
- [26] F. Nolde, J. Q. Qu, C. Kohl, N. G. Pschirer, E. Reuther, K. Mullen, *Chem. Eur. J.* **2005**, *11*, 3959–3967.
- [27] G. Sauerbrey, *Z. Phys.* **1959**, *155*, 206–222.
- [28] A. Darga, J. Kecht, T. Bein, *Langmuir* **2007**, *23*, 12915–12922.
- [29] a) M. Rauscher, T. Salditt, H. Spohn, *Phys. Rev. B* **1995**, *52*, 16855–16863; b) M. P. Tate, V. N. Urade, J. D. Kowalski, T.-C. Wei, B. D. Hamilton, B. W. Eggiman, H. W. Hillhouse, *J. Phys. Chem. B* **2006**, *110*, 9882–9892.

Received: July 7, 2008

Revised: October 16, 2008

Published online: January 2, 2009